Linear magnetoresistance due to sample thickness variations: Applications to aluminum

G. J. C. L. Bruls, J. Bass,* A. P. van Gelder, H. van Kempen, and P. Wyder†
Research Institute for Materials, University of Nijmegen, Toernooiveld, 6525 ED Nijmegen, The Netherlands
(Received 23 October 1984)

A model of transverse magnetoresistance (MR) in metals due to sample-thickness variations is presented. It predicts larger magnetoresistance then do previous models. The model is applied to magnetoresistance data on well annealed, polycrystalline aluminum plates which are wedge shaped, or which contain surface defects such as steps, grooves, or projections. For wedge-shaped samples or samples containing a surface step, the model predicts magnetically induced voltages which differ on opposite sides of the sample, and which are not strictly linear in magnetic field strength B. Both phenomena occur with the predicted magnitudes. For grooves or projections which extend completely across the width of the sample, the model predicts a MR which is linear in B (LMR) and directly proportional to both the groove (projection) depth (height) and the sample width. The data are found to be in quantitative agreement with prediction. The prediction and observation of a very large LMR for large surface defects provides at least a partial resolution of a disagreement in the literature concerning the magnitude of LMR in single-crystal Al samples when **B** is directed along the [110] crystallographic axis. Thermal magnetoresistance measurements are shown to be consistent with the electrical measurements. Measurements are also reported on (i) the angular variation of MR when **B** is rotated away from the perpendicular to the sample surface; (ii) MR for surface defects which extend only part way across the sample; and (iii) MR for surface defects in unannealed Al plates.

I. INTRODUCTION

Linear magnetoresistance (LMR) in simple metals such as K, Al, and In is a phenomenon which has puzzled physicists for decades. On very general grounds,[1] the magnetoresistance of a homogeneous uncompensated metal with no open orbits in k space should saturate with increasing magnetic field to a constant value ρ_s. There is continuing disagreement over whether the observed LMR is intrinsic or extrinsic. The most ably defended potential intrinsic source is Overhauser's charge-density-wave model (Ref. 2). Proposed extrinsic sources include magnetic-field nonuniformity along the sample length,[3] dislocations in the sample,[4] and the presence of volume defects (voids) in the sample.[5–7] Macroscopic voids have been shown to produce an LMR proportional to their volume fraction in the sample.[8,9] In carefully prepared samples, however, this volume fraction is too small to produce the observed LMR. Although surface defects were also previously suggested as a source of LMR,[6] extension of the volume-void theory of LMR to surface defects yields an LMR too small to explain published data. Moreover, the volume-void theory of Refs. 5–7 is only applicable to defects which are small with respect to sample dimensions, because the change in Hall field can be neglected in this case. For sample-thickness variations stretching across the whole width of a sample this approximation is no longer valid.

In a previous letter,[10] we showed that surface imperfections of this latter kind produce a transverse LMR which is larger than expected from the void theories. We showed also how these LMR can be understood quantitatively. In this paper, we provide further details of both our data and our model for surface-defect-induced LMR. The paper is organized as follows. In Sec. II, we first outline the volume-defect theory of LMR as background. We apply it to surface defects, and demonstrate its inadequacy. We then describe our new model and derive the equations needed to analyze our data. In Sec. III, we describe our experimental technique and procedures. In Sec. IV, we present and analyze our data. Section V contains a summary of the most important results, and our conclusions.

II. THEORY

We are interested in the transverse magnetoresistance ρ_{xx} of a sample whose thickness varies along the direction of an applied magnetic field $\mathbf{B}=B_z\hat{\mathbf{z}}$. We limit ourselves to consideration of a homogeneous, uncompensated metal with no open orbits. In the high-field limit, $\beta=\omega_c\tau\gg 1$, the transport equations for such a metal relating the electric field **E** to the current density **J** are

$$\begin{aligned} E_x &= \rho_s(J_x+\beta J_y)\ , \\ E_y &= \rho_s(-\beta J_x+J_y)\ , \\ E_z &= \rho_s J_z\ . \end{aligned} \tag{1}$$

Here $\omega_c=eB/\hbar c$ is the cyclotron frequency and ρ_s is the saturation magnetoresistance of the homogeneous metal. In Eqs. (1), E_i and J_i $(i=x,y)$ are functions of x, y, and z. As our measure of the LMR we use the dimensionless Kohler slope S:

$$S=\frac{1}{\rho_s}\left[\frac{\partial\rho(\beta)}{\partial\beta}\right]=\frac{1}{R_H}\left[\frac{\partial\rho(B)}{\partial B}\right],$$

where R_H is the high-field Hall constant and $\rho_s\beta=R_HB$.

The problem is to solve Eqs. (1) with the appropriate boundary conditions, subject to the constraint that current is conserved:

$$\nabla\cdot\mathbf{J}=0\,. \tag{2}$$

No general solution has been provided for samples of arbitrary shape and dimensions, but some limited solutions have been published.

Stroud and Pan[5] used an effective-medium approach to derive the LMR for elliptical inclusions of characteristic dimension d in the limits $\lambda\ll d\ll l$, where λ is the electronic mean free path, and l is a typical dimension of the sample. They found

$$S=\alpha f\,, \tag{3}$$

where f is the volume fraction of inclusions, and α is a constant equal to 0.49 for spherical nonconducting inclusions and 1 for long cylindrical voids parallel to the y axis. They did not calculate S for a long bar of rectangular cross section. If we use their calculation for the closest available approximation to our geometry, namely a half-cylinder at the surface of a sample, we obtain (with $\alpha=1$)

$$S=\frac{\alpha\pi c^2L_y}{2d_0LL_y}=\frac{\pi}{2}\left[\frac{c}{d_0}\right]\left[\frac{c}{L}\right]=f\,. \tag{4}$$

Here L is the length of the sample, L_y its width, d_0 its thickness, f is again the volume fraction, and c the radius of the cylinder. This result is independent of sample width and quadratic in c.

Sampsell and Garland[6] obtained Eq. (3) by directly integrating the power dissipated in the vicinity of the voids.

van Gelder[7] obtained exactly Eqs. (3) and (4) by a procedure we describe in more detail because of its relevance to our new model. He began from the inverted form of Eq. (1):

$$\begin{aligned}J_x&=\frac{1}{\rho_s(1+\beta^2)}\frac{\partial\phi}{\partial x}+\frac{-\beta}{\rho_s(1+\beta^2)}\frac{\partial\phi}{\partial y}\,,\\ J_y&=\frac{\beta}{\rho_s(1+\beta^2)}\frac{\partial\phi}{\partial x}+\frac{1}{\rho_s(1+\beta^2)}\frac{\partial\phi}{\partial y}\,,\\ J_z&=\frac{1}{\rho_s}\frac{\partial\phi}{\partial z}\,,\end{aligned} \tag{5}$$

where $E_i=\partial\phi/\partial i$ $(i=x,y,z)$. Equation (2) then gives

$$\frac{\partial^2\phi}{\partial x^2}+\frac{\partial^2\phi}{\partial y^2}+(1+\beta^2)\frac{\partial^2\phi}{\partial z^2}=0\,. \tag{6}$$

Equation (6) was reduced to a two-dimensional problem by averaging all quantities of interest over y:

$$\langle J_x\rangle=\frac{\int dy\,J_x(x,y,z)}{L_y}\,, \tag{7}$$

so that Eq. (5) remains valid for the averaged quantities $\langle(\partial\phi)/(\partial x)\rangle$, $\langle(\partial\phi)/(\partial y)\rangle$, but Eq. (6) becomes

$$\frac{\partial^2\langle\phi\rangle}{\partial x^2}+(1+\beta^2)\frac{\partial^2\langle\phi\rangle}{\partial z^2}+\frac{[\partial\phi/\partial_y]^{+}_{-}}{L_y}=0\,. \tag{8}$$

Here $[\partial\phi/\partial y]^{+}_{-}$ is the difference between $\partial\phi/\partial y$ on two opposite sides of a sample.

van Gelder then assumed that the third term on the right-hand side of Eq. (8) would become negligible as $L_y\to\infty$, which then leaves a totally two-dimensional problem. He also assumed that the averaged Hall field $\langle\partial\phi/\partial y\rangle$ was independent of x, and hence equal to the Hall field at large distances from the inclusion (or surface defect). This latter assumption was also explicitly made by Sampsell and Garland.

With these assumptions, van Gelder derived, by means of an appropriate transformation in the complex plane, exactly Eq. (4) for a cylindrical groove or projection, and the approximate equation

$$S\simeq\tfrac{1}{2}\left[\frac{c}{d_0}\right]\left[\frac{c}{L}\right]\ln\left[20.7\frac{a}{c}\beta\right] \tag{9}$$

for a rectangular groove (projection) of depth (height) c and length $2a$ along the x axis, oriented parallel to the y axis. For a square $(c=2a)$ groove this gives $S=\alpha f$, where α is a number of order unity which varies slowly (logarithmically) with magnetic field, and f is the volume fraction.

The agreement of all these calculations with each other leads us to believe that all are, in our geometry, effectively limited to the approximations $L_y=\infty$, and Hall field independent of x, as explicitly assumed by van Gelder.

The problem with all three calculations is that they yield results independent of L_y, and thus in fundamental disagreement with the data we describe below. We discovered the disagreement while using samples with $L_y=1.8$ mm. Figure 1 compares our experimental LMR for grooves in the 1.8-mm sample with the predictions of Eqs. (4) and (9), both of which are too small to explain the data. Since the predictions of Eqs. (4) and (9) were derived for samples with $L_y=\infty$, we tried a wider sample ($L_y=3.6$ mm) to see if the LMR would decrease in magnitude. Instead, they increased! Additional measurements with a 0.7-mm-wide sample revealed that the LMR were proportional to L_y. This result led us to reformulate the theory to generate a dependence on L_y.

Instead of averaging over y as in Eq. (7), we average over z. As we will see, for our geometry this leads to a solvable set of differential equations of two variables without having to assume that the Hall field is independent of position. This latter release of constraint gives rise to our effect. The averaging is defined as follows:

$$\begin{aligned}\langle E_i\rangle&=\frac{1}{d}\int_0^d E_i\,dz\,,\\ \langle J_i\rangle&=\frac{1}{d}\int_0^d J_i\,dz\equiv\frac{K_i}{d}\,.\end{aligned} \tag{10}$$

Here d is the sample thickness, and $i=x,y$. Since there is continuity of current in three dimensions [see Eq. (2)], there must also be continuity of averaged current in two dimensions:

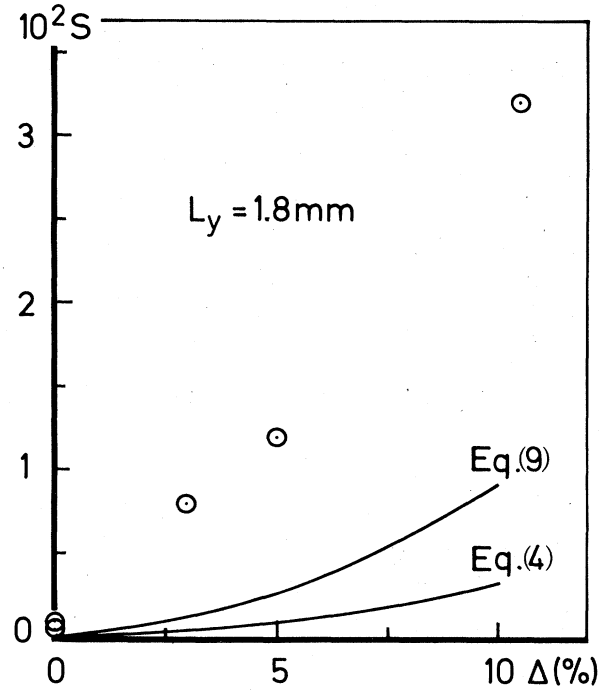

FIG. 1. Measured experimental LMR (open circles), expressed in Kohler slope S, of grooves of different depth in samples of width $L_y = 1.8$ mm, compared with the predictions of the volume fraction theories [Eqs. (4) and (9)].

$$\frac{\partial K_x}{\partial x}+\frac{\partial K_y}{\partial y}=0 \tag{11}$$

because no current can be lost. This means that a function F can be found such that $K_x=\partial F/\partial y$ and $K_y=-\partial F/\partial x$. The transport equations (1) can then be rewritten as

$$\langle E_x\rangle=\left[\frac{\rho_s}{d}\right]\left[\frac{\partial F}{\partial y}-\beta\frac{\partial F}{\partial x}\right],$$
$$\langle E_y\rangle=\left[\frac{\rho_s}{d}\right]\left[-\beta\frac{\partial F}{\partial y}-\frac{\partial F}{\partial x}\right], \tag{12}$$

where $\langle E_i\rangle$, $(\partial F/\partial i)$, and d depend on x and y. The problem is again reduced to two dimensions, since $\langle J_z\rangle$ and $\langle E_z\rangle$ are zero.

In a constant magnetic field the three-dimensional electric field is rotation free, but this need not be the case for the two-dimensional averaged field. The rotation of the averaged field can be rewritten as

$$\nabla\times\langle\mathbf{E}(x,y)\rangle=\frac{\partial d}{d\,\partial x}\gamma_y\langle E_y(x,y)\rangle-\frac{\partial d}{d\,\partial y}\gamma_x\langle E_x(x,y)\rangle\ , \tag{13}$$

where γ_i $(i=x,y)$ is the fractional deviation of the field E_i at the surface from its averaged value within the sample:

$$\gamma_i(x,y)=[E_i(x,y,d)-\langle E_i(x,y)\rangle]/\langle E_i(x,y)\rangle\ . \tag{13a}$$

Inserting (12) into (13) we get

$$\frac{\partial^2 F}{\partial x^2}+\frac{\partial^2 F}{\partial y^2}-\frac{1}{d}\left[\frac{\partial d}{\partial x}\right](1+\gamma_y)\left[\frac{\partial F}{\partial x}+\beta\frac{\partial F}{\partial y}\right]+\frac{1}{d}\left[\frac{\partial d}{\partial y}\right](1+\gamma_x)\left[\beta\frac{\partial F}{\partial x}-\frac{\partial F}{\partial y}\right]=0\ . \tag{14}$$

For a groove or projection extending completely across the sample, $\partial d/\partial y=0$, and the last term on the left-hand side in Eq. (14) is identically zero. It seems unlikely that γ_y will be larger than Δ, the fractional change in sample diameter at point x, and it may well be considerably smaller. If we approximate γ_y as Δ, then neglecting it will make an error in the second term from the right of Eq. (14) of only Δ. In our case, this will be less than 11%, which is the largest Δ used for quantitative studies. Since 11% is comparable to our typical overall experimental uncertainty, we neglect γ_y. This amounts to assuming the rotation of the averaged field to be zero. With $(\partial d/\partial y)/d=0$, $\gamma_y=0$, and $(\partial d/\partial x)/d=1/a$ we get from Eq. (14)

$$\frac{\partial^2 F}{\partial x^2}+\frac{\partial^2 F}{\partial y^2}-\frac{1}{a}\left[\frac{\partial F}{\partial x}+\beta\frac{\partial F}{\partial y}\right]=0\ . \tag{15}$$

Interestingly, this is the same equation as Bate and Beer[11] derive for the influence of a conductivity gradient on the magnetoresistance of semiconductors, with carrier-concentration gradient taking the place of thickness variation. In hindsight this is not so surprising since both thickness variation and carrier-concentration gradients cause changes in Hall field. A third cause for change in Hall field is inhomogeneity of the magnetic field. Again this leads to the same equations and phenomena (see, for instance, Ref. 3).

Equation (15) can be solved in closed form if a is taken to be constant, which corresponds to a wedge-shaped sample of thickness $d=d_0\exp(x/a)$. The solutions are

$$K_y=-\frac{\partial F}{\partial x}=0\ ,$$
$$K_x=\frac{\partial F}{\partial y}=I(\beta/2a)\frac{\exp(\beta y/a)}{\sinh(\beta L_y/2a)}\ , \tag{16}$$

where I is the total current.

If we choose axes down the middle of the sample, then what we measure are the voltages $V_x(\pm L_y/2)$ at the sides of the sample $(y=\pm L_y/2)$ between the positions $x=0$ and $x=L$ (see Fig. 2). Calculating E_x and integrating from 0 to L gives

$$V_x(\pm L_y/2)=\frac{I\beta\rho_s\exp(\mp\beta L_y/2a)}{2d_0\sinh(\beta L_y/2a)}\Delta\ , \tag{17}$$

where

$$\Delta=[1-\exp(-L/a)]=(d_1-d_0)/d_1$$

is the relative thickness variation of the wedge-shaped sample (for our sample, 10%). The difference between these two voltages,

$$V_x(-L_y/2)-V_x(+L_y/2)=(I\rho_s\beta\Delta)/d_0\ ,$$

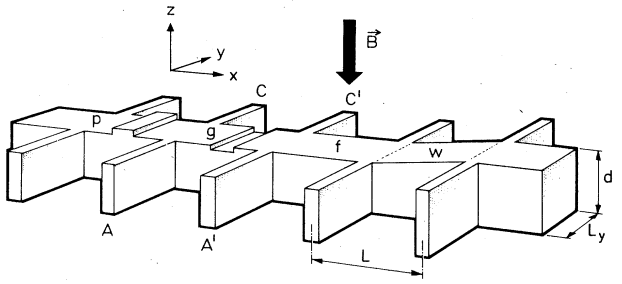

FIG. 2. Composite sample of width L_y, thickness d, and length between potential leads, L. Shown are a flat part (f), a wedge-shaped part (w), a part with a projection (p), and a part with a groove (g). Voltages are measured over pairs of potential contacts, e.g., AA' and CC'.

is just equal to the difference in Hall voltage between the place on the sample having thickness d_1 and the place having thickness d_0. Our mechanism thus works as follows: The requirement that the (averaged) field is rotation free forces differences in Hall voltage caused by thickness variations to appear along the length of the sample, thereby producing a large LMR.

Finally, we define

$$\rho_{\pm}=V_x(\mp L_y/2)(d_0L_y/LI) ,$$

and obtain

$$\rho_{\pm}(\text{wedge})=(\rho_s\beta L_y\Delta/2L)\frac{\exp(\pm\beta L_y/2a)}{\sinh(\beta L_y/2a)} , \tag{18}$$

$$\frac{\rho_+ +\rho_-}{2}=(\rho_s\beta L_y\Delta/2L)\coth(\beta L_y/2a) . \tag{18a}$$

It is gratifying to note that the $\rho_{\pm}$ from Eq. (18) satisfy the consistency condition that their average, $\rho=(\rho_+ +\rho_-)/2$, from Eq. (18a) is just equal to the true resistivity defined via the power dissipation in the sample. This is seen by substituting our averaged quantities into the power integral $P=\int \mathbf{J}\cdot\mathbf{E}\,dv$, which then becomes $P=\int \mathbf{K}\cdot\langle\mathbf{E}\rangle dx\,dy$. Inserting the $\mathbf{K}$ and $\langle\mathbf{E}\rangle$ obtained from Eqs. (12) and (16) and computing the integral yields a ρ which is equal to the right-hand side of Eq. (18a). The fact that the true resistivity is equal to the average of the "resistivities" measured at opposite sides of a sample follows more generally for both the wedge and other surface defects from the consideration that the dissipation is equal to the integrated Poynting vector over the sample surface, which can be shown to involve only integration over the surfaces $y=-L_y/2$ and $y=L_y/2$.

We can derive an LMR appropriate to a sharp step by letting $a\to 0$ in Eq. (18) while holding Δ constant. This yields the asymmetric ρ_+ and ρ_-:

$$\rho_+(\text{step})=\frac{\rho_s\beta L_y\Delta}{L}+\rho_s , \tag{19}$$

$$\rho_-(\text{step})=0+\rho_s , \tag{19a}$$

where, since the contribution to $\rho_{\pm}$ from the step is localized to the region of the step, we have added in the ρ_s due to the flat parts of the sample. This extra ρ_s makes no contribution to the slope of the LMR. The average resistivity for the step, $\rho_{\text{step}}=(\rho_+ +\rho_-)/2$, is then

$$\rho_{\text{step}}=\frac{\rho_s\beta L_y\Delta}{2L}+\rho_s \quad \text{or} \quad S_{\text{step}}=\frac{L_y\Delta}{2L} . \tag{20}$$

It is also possible to find an analytical solution for the problem of a steep step. Bate, Bell, and Beer[12] give a series solution for the analog problem of a steplike change in carrier concentration in a semiconductor. However, this series solution does not work well because of a singularity in the current distribution (see Fig. 3). This current pattern and the resulting asymmetric resistivities were computed by one of us (Ref. 7) by means of a complex-function method. The resistivities for both sides of the sample are

$$\frac{\Delta\rho^+}{\rho}=\frac{L_y}{L}\frac{2}{\pi}[\Psi(\tfrac{1}{2})-\Psi(\phi/\pi)] , \tag{21}$$

$$\frac{\Delta\rho^-}{\rho}=\frac{L_y}{L}\frac{2}{\pi}[\Psi(\tfrac{1}{2})-\Psi(1-\phi/\pi)] . \tag{21a}$$

Here L_y is the width of the sample, L is the distance between potential contacts, Ψ is the digamma function, see, for instance, Ref. 13, and

$$\phi=\frac{\pi}{2}-\arctan\left[\beta\frac{\Delta}{2}\right] ,$$

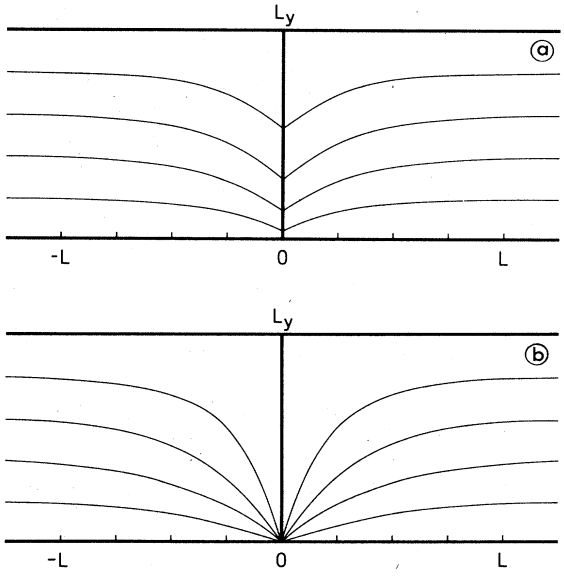

FIG. 3. Current lines near a steplike variation in sample thickness, in Hall constant, or in magnetic-field strength. The length (from $-L$ to $+L$) over which the current deviates appreciable from a homogeneous current distribution is comparable to the width of the sample L_y. Panel (a) shows the current pattern for $\beta\Delta\simeq 5$, which lies in the middle of our experimental range. Panel (b) shows the pattern for $\beta\Delta\geq 20$, at which point the lines converge to within about 1% of the sample width.

where $\beta \equiv \omega_c \tau$ is the product of cyclotron frequency and scattering time and Δ is the previously defined relative thickness variation.

In Ref. 13 one can find suitable series expansions which for $\beta(\Delta/2) \geq 1$ give to good accuracy

$$\frac{\Delta\rho^+}{\rho} = \frac{L_y}{L}(\beta\Delta - 0.9) , \tag{22}$$

$$\frac{\Delta\rho^-}{\rho} = \frac{L_y}{L}(-0.9) , \tag{22a}$$

and for the average of the two

$$\frac{\Delta\langle\rho\rangle}{\rho} = \frac{L_y}{L}\left[\beta\frac{\Delta}{2} - 0.9\right] . \tag{23}$$

In these equations we have approximated $(4\ln 2)/\pi$ by 0.9. This gives a linear magnetoresistance with a Kohler slope given again by Eq. (20). So the analytical calculation differs from the approximate one only by a slight renormalization of ρ_s, which does not affect the Kohler slope. This agreement gives confidence in our solutions and in our mechanism.

A sample with a groove or a projection is approximated by two steps of opposite slope bounded by flat pieces. Placing two such steps in series has the consequence that, seen over the whole sample, the asymmetry vanishes. The resistivity is just twice the average contribution of a single step, plus the ρ_s due to the flat parts of the sample

$$\rho(\beta) = \frac{\rho_s \beta L_y \Delta}{L} + \rho_s \quad \text{or} \quad S = \frac{L_y}{L}\Delta . \tag{24}$$

S is thus linearly dependent on Δ, the relative depth (height) of the groove (projection), and also on the width of the sample, L_y, but not on the volume fraction f. For a sample with $L_y/L = 1$, and a single groove of relative depth $\Delta = 1\%$, we find $S = 10^{-2}$, which is already larger than many reported values in the literature ($S = 10^{-3}$–10^{-1}).[14,15]

In deriving the above equations, we have assumed that the surface defects are the only source of LMR. In fact, some LMR is seen even with "flat" samples. In the spirit of Eqs. (21)–(24), such an additional LMR should probably be added to ρ_s to properly account for the contribution due to the real flat portions of the sample. In presenting our data, we have chosen to treat this issue from the alternative point of view that the LMR due to flat pieces should be subtracted from the raw data before comparison with Eqs. (19)–(21).

For the wedge, which extends over the entire sample length between the potential leads, ρ_s is already contained in Eq. (18) as the limit of $\rho_\pm$ as $\beta \to 0$. It is thus less clear how to include any "additional LMR," especially in ρ_+ and ρ_- separately. From the physical changes in current pattern associated with our model, which involves a bunching up of current lines on one side of the wedge, we infer that effects of any additional LMR will be magnified on that side of the wedge relative to the other side. We have thus subtracted from ρ_+ and ρ_- the "flat-surface LMR" multiplied with the ratio of computed and average current density in correcting the data for the wedge to be discussed below.

We can also make a similar argument for the LMR due to "volume-defect theory," which involves different current distortions than those in our model. The simplest assumption to make is that the effects of the two different types of distortion simply add together. For completeness, we present our data both with and without such corrections.

Since our samples have residual resistance ratios (RRR's) of 10.000–20.000, corresponding to mean free paths of electrons in zero magnetic field of $\lambda \simeq 0.2$–0.4 mm, which are comparable to the sizes of our samples and any grooves or projections, one might wonder whether an essentially classical and macroscopic model such as we have developed is appropriate for describing our data. We believe that it is, for the following reason. A fundamental assumption of our analysis is that the averaged electric fields and current densities of interest are functions only of the local position (x,y). In zero magnetic field, a long electronic mean free path vitiates this assumption, because the electrons carry with them information from their last collision, which occurred a long distance (λ) away. However, in high magnetic field, $\omega_c\tau \gg 1$, an electron is constrained to a region of order $\lambda/\omega_c\tau$ in the plane perpendicular to the magnetic field. In our case, fields of 2 to 5 T along the z axis give $\omega_c\tau \simeq 50$–400 for the different sample purities, so that electrons are constrained to regions of $\lesssim 0.003$ mm in the x-y plane. These distances are much smaller than any dimension of our samples. The electrons travel over larger distances in the z direction, but we do not care about the details of their motion in this direction, because our model involves an average over the z-axis properties of the quantities of interest. We thus conclude that our model should be applicable to our experimental data.

III. EXPERIMENTAL DETAILS

The samples were prepared from high-purity polycrystalline Al plates of 2 mm thickness obtained from Vereinigte Aluminium Werke.[16] As received, the Al had a residual resistance ratio [RRR $= R(300\text{ K})/R(4.2\text{ K})$] of $\simeq 10.000$. After annealing at 500 °C for a few hours in vacuum or argon, the RRR increased to $\simeq 20.000$. Spark erosion was used to form bars of different widths, L_y, with regularly spaced arms for potential contacts on both sides of the sample. Figure 2 shows a composite sample. A typical sample was ≥ 5 cm long and divided into five or ten equal parts by the potential arms. Between some pairs of arms were machined projections (p) and between some pairs' grooves (g). Each sample also contained one or more flat, untreated regions (f) to serve as controls. To minimize damage, the grooves or projections were initially cut using spark erosion. Later, a milling machine was used to get more uniform grooves with sharper edges. No significant differences were found between results obtained with the two techniques. Usually, the grooves or projections extended over the entire width of the sample, but some tests were made with grooves cut only part way across. The behavior of the magnetoresistance for steps (not shown) and wedge-shaped (w) portions of the sample were also examined.

Measurements were made on both annealed and unannealed samples, with results which were qualitatively similar, but differed in some details as described below. In the unannealed state, the samples contained large numbers of small, randomly oriented grains. After annealing, there were typically only a few grains between pairs of potential leads. The general agreement between results for different samples indicates that the detailed grain structure was not an important factor in the observed LMR.

Conventional four-probe measurements of transverse LMR were made, usually with the magnetic field **B** of the split-coil superconducting solenoid oriented perpendicular to the plane of the sample arms. In a few cases, the LMR was measured for the entire angular range from 0° (**B** perpendicular to the plane of the arms) to 90° (**B** parallel to the plane of the arms). To test for sensitivity of the LMR to the exact orientation of the sample, the effect of small misalignments of the sample normal with respect to the magnetic field was regularly checked. For defects extending across the whole width of the sample such misalignments had little effect. We also checked that small displacements of the sample up or down out of the middle of the solenoid had little effect on the data. Larger displacements, which brought the sample to a region of significant field inhomogeneity, produced results similar to those reported by Gostishchev *et al.*[3]

The measuring currents were normally chosen to make the current density through the sample about 0.3 A/mm^2, and occasional checks were made that the data were independent of the measuring current. We regularly checked potential differences on both sides of the sample (e.g., $V_{AA'}$ and $V_{CC'}$ in Fig. 3),[17] and except for the wedge-shaped samples and steps, for which $V_{AA'}$ and $V_{CC'}$ were very different, the two potential differences were always nearly equal. When a slight difference appeared, the two values were averaged. The data to be presented were also the result of reversing both current and field and taking appropriate averages. Reversing the current rarely led

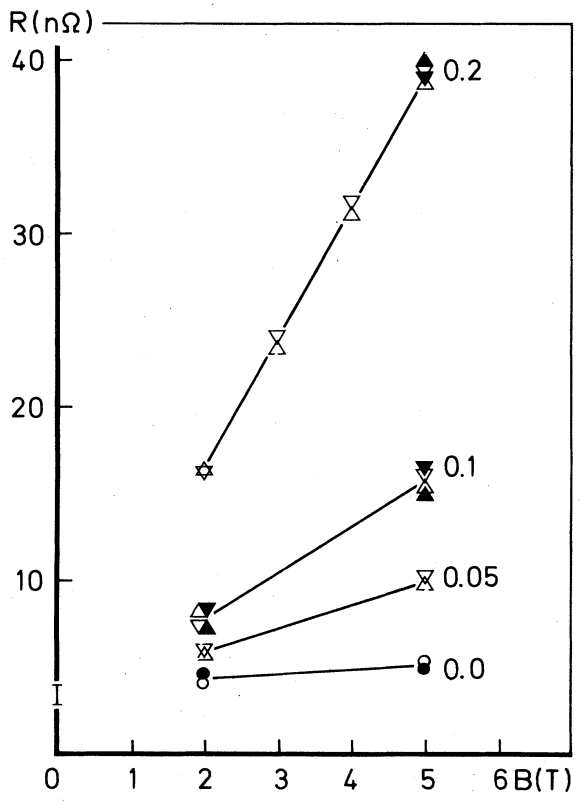

FIG. 4. Measurement of resistance as a function of field for three grooves of different depth and two flat regions on an annealed 4-mm-wide sample. The numbers shown are values of Δ. Upright and inverted triangles indicate results for opposite-field directions. Solid and open symbols indicate measurements on opposite sides of the sample (e.g., *AA'* and *CC'* in Fig. 2, respectively). The circles which describe data for the flat regions represent averages after field reversal. The two flat pieces gave results too close together to separate on this graph.

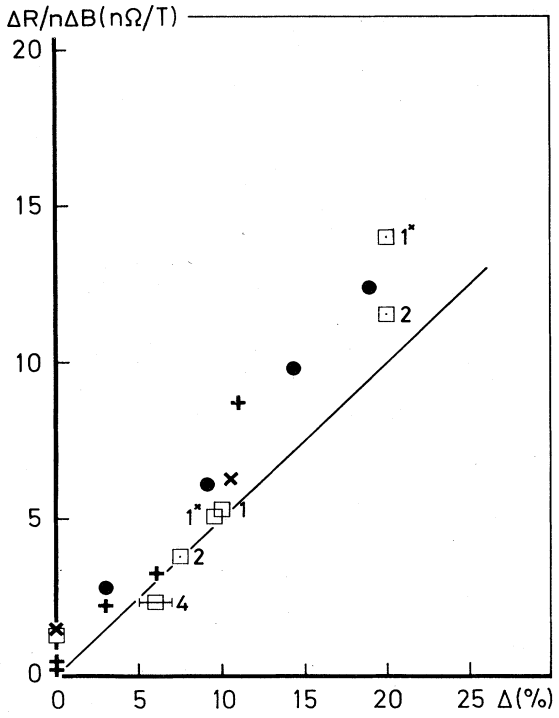

FIG. 5. Slope of LMR for grooves and projections of different depth (height), on annealed and unannealed samples, divided by the number of grooves (projections) between voltage contacts. The solid line is the theoretical calculation from Eq. (24). The solid circles indicate data for a sample containing projections, in which the projection height was sequentially reduced. The pluses and crosses represent data for two annealed samples containing grooves (pluses) or projections (crosses), respectively. The open squares represent data for an unannealed sample containing multiple grooves (the number of grooves is specified at each symbol), with different depths for each different set of grooves. Two grooves (indicated by asterisks) were made unusually long (3 mm versus a normal 1 mm) along the x direction to see whether such extra length would affect the LMR. None of the data shown in this figure have had the LMR for flat pieces subtracted. The LMR's for flat pieces on each of the samples (except for the solid circles where no flat piece was measured) are indicated on the ordinate axis at $\Delta=0$.

to significant asymmetry, and field-reversal asymmetries were typically less than 10—20%. Voltages were measured with a sensitivity and noise of about 10^{-9} V using a Tekelec digital voltmeter,[18] the output of which was displayed on a strip-chart recorder so that noise and thermal drift could be averaged out where necessary.

Figure 4 shows resistance as a function of field for three grooves of different depths, and two flat regions, on an annealed 4-mm-wide sample. This figure illustrates (a) that above about 2 T the magnetoresistances are linear in B; (b) that the deeper the groove, the larger the LMR, and that the background LMR for flat regions are smaller than the LMR for grooves and nearly the same for different flat regions on a given sample; and (c) that the differences between $V_{AA'}$ and $V_{CC'}$ are small for both grooves and flat regions.

To test whether damage introduced by spark erosion was the source of our observed LMR, an unannealed sample was first fabricated with relatively long projections and then spark-planed down in steps so that the projections became shorter and shorter. The solid circles in Fig. 5 show that the LMR for this sample decreased approximately linearly with decreasing projection height. Figure 5 also contains for comparison some data for annealed samples (pluses and crosses) with grooves instead of projections, to demonstrate that the LMR's obtained are consistent with those for the projections. We conclude that the LMR's we see are due primarily to the presence of grooves or projections and not to damage introduced during fabrication. Finally, Fig. 5 also contains data for an unannealed sample (open squares) containing multiple grooves and grooves which are longer (3 mm) in the x direction than the typical ones (1 mm). We see that the LMR's are approximately proportional to the number of grooves and independent of groove length. If we subtract the LMR for flat pieces from each of the samples in Fig. 5, we find that the data for the unannealed sample fall below those for the annealed samples. We consider this behavior further in Sec. IV C below.

IV. DATA AND ANALYSES

This section is divided into three parts. In subsection A, we describe measurements of the Hall voltage, V_y, which are basic to our model of surface-defect LMR. In subsection B, we present that portion of our data which can be quantitatively explained by our model, namely the LMR for annealed samples which are wedge shaped or plane parallel with grooves, projections, or steps, all with the magnetic field directed perpendicular to the plane of the sample arms. We also describe measurements with the field parallel to the plane of the arms, and use these measurements both to demonstrate that the average electric field in the sample is independent of the strength of the magnetic field, and to resolve a contradiction in the literature concerning LMR in single-crystal Al when the magnetic field is directed along the [110] crystal axis. We show also that thermal LMR behaves the same as electrical LMR in these parallel and perpendicular geometries. In subsection C, we describe results which are less well understood, primarily the angular variation of LMR for large projections, LMR in unannealed samples, and LMR due to grooves or projections which extend only partially across the sample.

A. The Hall voltage and LMR

As indicated in Sec. II, previous models assumed that the Hall voltage V_y is independent of x, whereas in our model it varies inversely with sample thickness d. The irrotationality of the averaged electric fields causes these differences in Hall voltage to appear along the current direction as a LMR. We tested this prediction using a sample in which the potential leads were in the middle of portions of the sample having different thicknesses. Figure 6 compares the differences in the Hall voltage ΔV_y with the LMR voltages V_x appearing across the same sample, for several different values of $\Delta=(d_1-d_0)/d_1$. No corrections or adjustments are made. The approximate agreement between ΔV_y and V_x validates the foundation of our model.

B. Data well described by the model

Our model can be solved exactly for an exponential wedge, giving Eq. (18). This equation, which we now show contains no adjustable parameters, predicts that ρ_+ and ρ_- vary not strictly linear with B and are very different from each other. In Eq. (18), Δ, L_y, L, and a are all directly measurable on the sample, and ρ_s and β are related via $\rho_s\beta=R_HB$. It is thus necessary only to determine ρ_s.

For magnetoresistance in samples of uniform thickness, there are two field regimes: (a) "low field" ($\beta\ll1$), where $\rho\simeq\rho_0$, and (b) "high field" ($\beta\gg1$), where $\rho\simeq\rho_s$. For our wedge in contrast, there are three field regimes: (a) "low field," $\beta\ll1$, where $\rho=(\rho_++\rho_-)/2\simeq\rho_0$; (b) "intermediate field," $\beta\gg1>\beta L_y/2a$, where $\rho\simeq\rho_s$; and (c) "high field," $\beta L_y/2a\gg1$, where ρ varies linearly with β. For our wedge, $a=100$ mm and $L_y=1.33$ mm, so that at our lowest field of 1 T we are in the "intermediate-field" regime. We thus take for R_s, the "saturation resistance" of

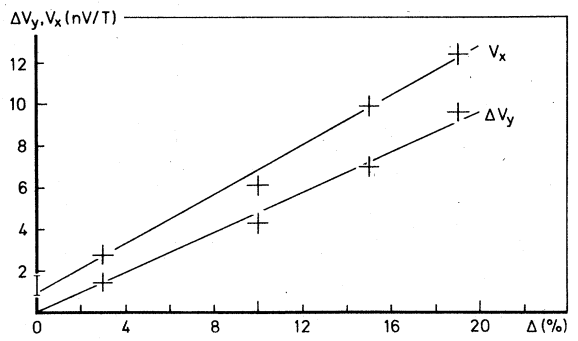

FIG. 6. Comparison, for a projection, between the difference in Hall voltage ΔV_y and the LMR voltage V_x as a function of the fractional projection height $\Delta=(d_1-d_0)/d_1$. Here ΔV_y is the difference between the Hall voltages measured along the projection and along a flat portion of the sample, and V_x is the LMR voltage measured across the projection.

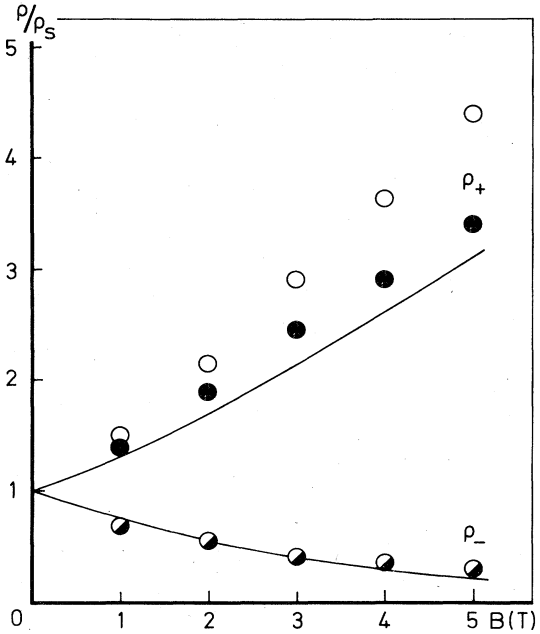

FIG. 7. ρ/ρ_s data for a wedge-shaped sample, together with the theoretical prediction of Eq. (18) (solid curve) using $\beta=44/\mathrm{T}$, $R_s=13$ nΩ, and $a=10$ cm. The open circles represent uncorrected data and the solid circles corrected data (see text).

our sample, the average value of our measurements of R_- and R_+ at $B=1$ T, and then convert R_s into ρ_s using the geometric factor of our sample derived from the ratio of the known room-temperature resistance of our wedge and the specific resistivity of aluminum. From this ρ_s we obtain $\beta=44/\mathrm{T}$ which was used to calculate the curves of Fig. 7.

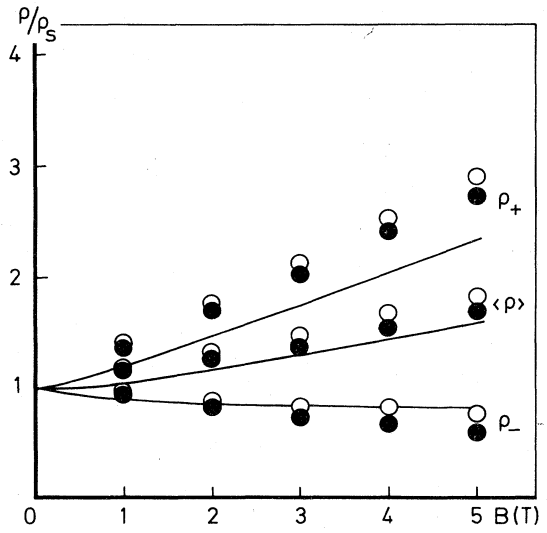

FIG. 8. Asymmetric resistivities and their average for a single sharp step, corrected (solid circles) and uncorrected (open circles) for residual LMR of flat pieces. The solid lines are the predictions from Eqs. (21) and (21a) using $\beta=15.6/\mathrm{T}$ determined from the RRR for this sample.

If the characteristic length a of the exponential is large, then for a sample of length $L \ll a$, Eq. (18) will apply with good accuracy to a linear wedge, which is easier to fabricate than an exponential wedge. Figure 7 compares the prediction of Eq. (18) (solid curves) with data for a linear, wedge-shaped sample. The open symbols represent uncorrected data. The solid symbols show the same data after correction according to the procedure described just after Eq. (24). The predicted curves are in good agreement with the corrected data and in reasonable agreement with the uncorrected data.

For a single sharp step, we have the prediction of Eqs. (21) and (21a). Figure 8 shows data for a single step (with and without flat-piece-LMR subtracted) compared to this prediction. Again the prediction is verified. As expected, the averaged values for the two sides of the sample yield a

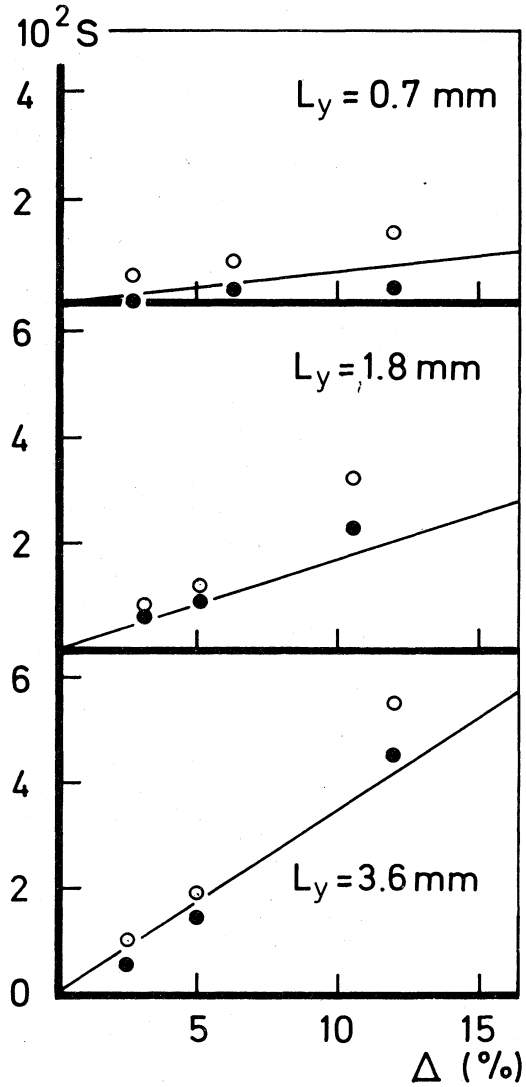

FIG. 9. Kohler slope S versus thickness variation Δ for samples of width 0.7, 1.8, and 3.6 mm. Open symbols are for uncorrected data. Solid symbols are the data with the residual LMR of flat control pieces and the LMR due to volume-defect theory subtracted as discussed in Sec. II. The solid lines are predictions from Eq. (24).

LMR of about half that expected for a groove (or projection) of the same depth (height).

For groove or projection, the high-field prediction is given by

$$S=\frac{L_y}{L}\Delta\ , \tag{25}$$

where $\Delta=(d_1-d_0)/d_{11}$ is the fractional change in thickness due to the groove or projection.

For a single groove (projection) we thus expect S to be proportional to Δ for fixed L_y. Figure 9 shows S versus Δ for three different groove depths in samples of width 0.7, 1.8, and 3.6 mm, respectively. The solid symbols are data corrected for both the residual magnetoresistance of flat control pieces and the LMR due to "volume-defect" theory as described in Sec. II. The open symbols are uncorrected data. The sizes of the symbols indicate their uncertainties due to uncertainties in groove depth and shape, and in the measurements of resistivities and determination of LMR slope. The straight lines are calculated from Eq. (25). These lines generally agree better with the corrected data, but are in reasonable agreement with the uncorrected data also.

For fixed groove depth, Eq. (24) predicts that S will be proportional to the sample width L_y. Figure 10 shows S versus L_y for three groove depths. Again, solid symbols are corrected data and open symbols are uncorrected. The straight lines are the predictions of Eq. (25). As in Fig. 9, the lines agree better with the corrected data, but are also in reasonable agreement with the uncorrected data.

As illustrated in Fig. 5, the observed LMR are essentially the same for projections as for grooves of the same height (depth), the LMR are independent of groove length along the sample, and the LMR are approximately linear in the number of grooves per unit length of the sample. We thus conclude that our data are in quantitative agreement with Eq. (25), which contains no adjustable parameters.

Up until now, we have examined data for small Δ, i.e., $\Delta\leq 11\%$, which is where we expect Eq. (25) to be valid. If Δ is allowed to increase further, then since $\Delta=(d_1-d_0)/d_1$, its limiting value is unity. This yields a limiting value for S of $S=L_y/L$. While we do not expect this limiting value to be quantitatively accurate, it is still worthwhile to examine its applicability experimentally.

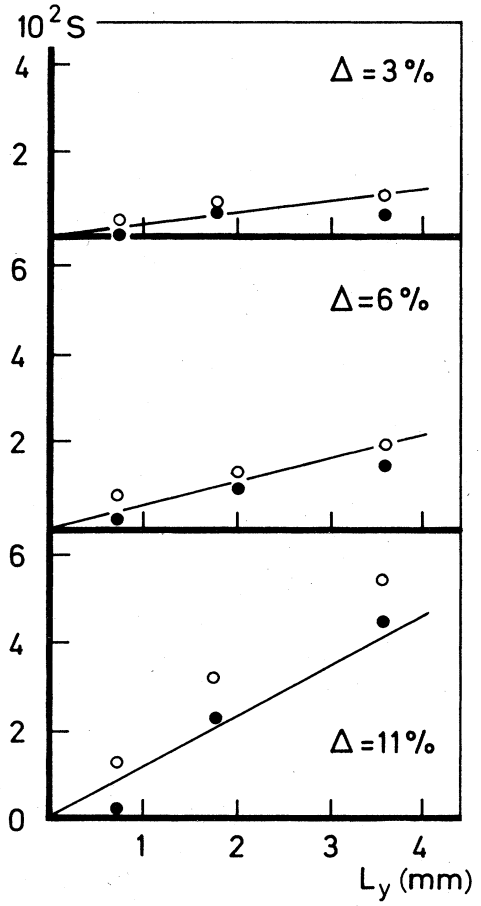

FIG. 10. Kohler slope S versus sample width L_y for three different groove depths. Open symbols are for uncorrected data. Solid symbols are the data with the residual LMR of flat control pieces and the LMR due to volume-defect theory subtracted. The solid lines are predictions from Eq. (24).

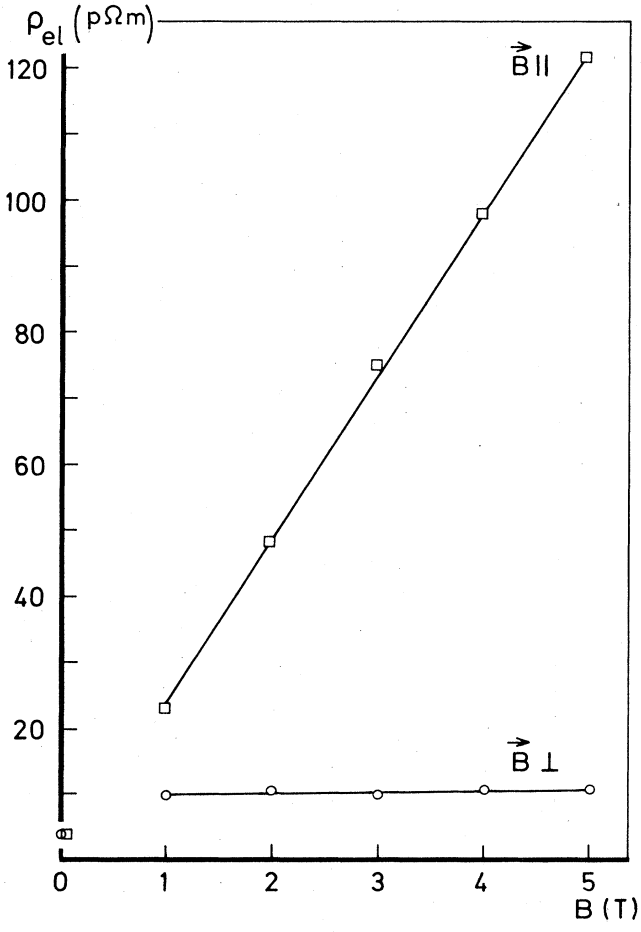

FIG. 11. The electrical resistivity ρ_{el} for a sample plate with no deliberately introduced defects. $\mathbf{B}_\perp$ indicates a field directed perpendicular to the sample and to the plane of the arms (see Fig. 2). $\mathbf{B}_{||}$ indicates a field directed along the arms.

The easiest way to simulate a large Δ is merely to rotate a sample by 90° so that the magnetic field points along the potential arms rather than perpendicular to the plane of the arms. This is not quite the same as having long projections or deep grooves in the proper geometry, since now the voltage is being measured on arms which point along the field direction. However, as we will now see, the results are similar to what is expected for the proper geometry.

Figure 11 shows the magnetoresistivity for a sample containing no deliberately introduced surface defects, with the field oriented both in and perpendicular to the plane of the arms. With the field perpendicular to the plane of the arms we see only the small LMR appropriate to a flat sample. With the field along the arms, however, we see a much larger LMR, with a value of S about half of L_y/L, the upper bound indicated above. The magnitude of this LMR is about the same on the two sides of the sample and also approximately symmetric under field and current reversal.

To see whether or not the behavior shown in Fig. 11 was associated solely with electrical magnetoresistivity, the thermal magnetoresistivity $\rho_{th}(B)$ was measured on a sample of the same shape,[19] prepared from the same Al plate as the one used for Fig. 11. Data for parallel and perpendicular fields are shown in Fig. 12. For parallel fields, where the effect is large, it is possible to calculate the Wiedemann-Franz ratio, $(1/T)[\rho_{el}(B)/\rho_{th}(B)]$, using the two linear slopes. Its value of $(2.2\pm0.2)\times10^{-8}$ $(V/K)^2$ is in good agreement with the Lorenz number 2.44×10^{-8} $(V/K)^2$.

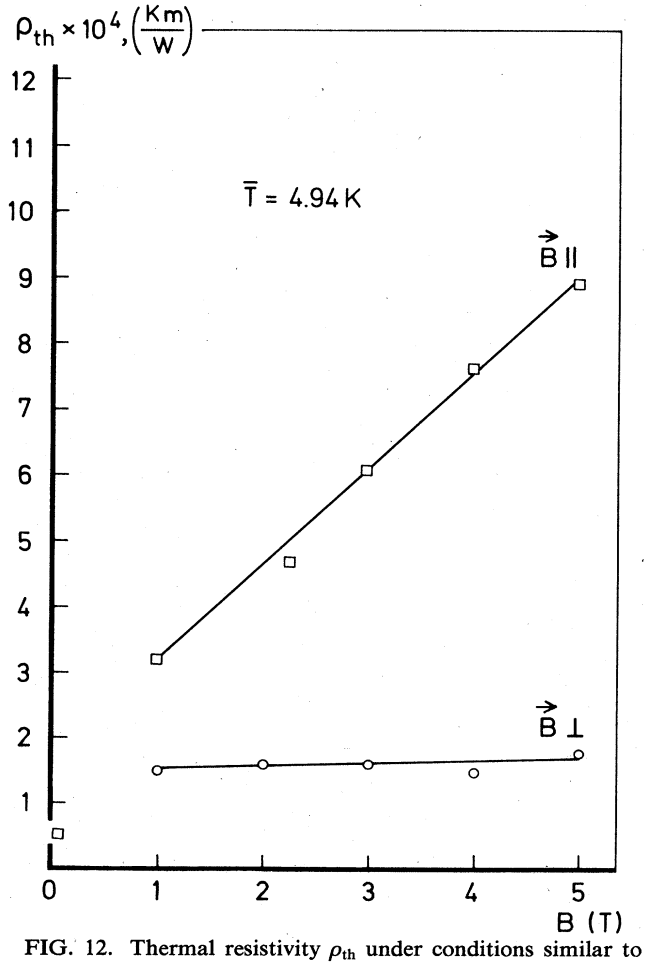

FIG. 12. Thermal resistivity ρ_{th} under conditions similar to those in Fig. 11.

We take this consistency check, plus the fact that S for the electrical LMR is comparable to the upper bound of Eq. (25), as additional evidence for the basic validity of our model. We can also use this geometry, and these results, to study further the fundamental physics underlying surface LMR.

It is easily demonstrated that the average electric field throughout the entire sample should be independent of the magnitude of the magnetic field B, provided that ρ_s is itself independent of B. We begin with the first of Eqs. (1),

$$E_x=\rho_s(J_x+\beta J_y)\ . \tag{1}$$

If we average this equation over the entire sample volume, we find

$$\langle E_x\rangle=\rho_s\langle J_x\rangle\ , \tag{26}$$

since $\langle J_y\rangle=0$. Because we maintain $\langle J_x\rangle$ constant as we increase the magnetic field, Eq. (26) predicts that $\langle E_x\rangle$ will be independent of magnetic-field strength B. This result is not only valid for **B** perpendicular to the plane of the sample arms (where indeed we observe a nearly constant ρ_s with $S\simeq10^{-3}$ in well-annealed samples with no deliberately introduced surface defects), but also for **B** parallel to the arms (where we observe a huge LMR with $S>10^{-1}$). From Eq. (26) we must infer for **B** parallel to the arms that the large electric fields giving rise to the huge LMR observed in the body of the sample must be balanced off by large oppositely directed fields in the arms.

To search for such a field, we attached potential leads across one arm of the sample as indicated in the inset of Fig. 13, and used these leads to measure the potential differences across this arm as a function of the magnitude of B. For B directed perpendicular to the plane of the

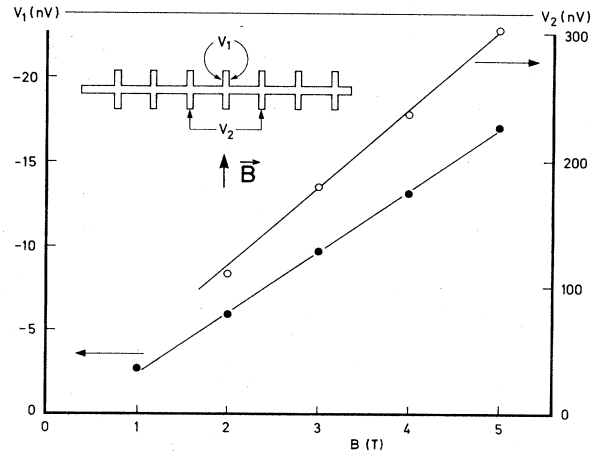

FIG. 13. Voltage V_1 (across a sample arm) and V_2 [between two different sample arms (see inset)] as functions of magnetic field strength B. Note that the data for V_1 and V_2 have opposite signs.

arms, no potential difference was observed. However, for **B** in the plane of the arms, we obtained the results shown in Fig. 13; the potential difference V_1 across the single arm increased linearly with B and was of opposite sign to the potential V_2 between two different arms. We measured V_1 at four different distances from the body of the sample, and found that it decreased with increasing distance from the sample. To estimate the magnitude of the average negative field in the arms, we drew a smooth curve through the data for the potentials in the arm for a fixed B, and then used this curve to roughly integrate the field in the arm. We found a total field in the arms which balanced off the positive field in the body of the sample to within our experimental uncertainty. The data thus confirm the expectation that $\langle E_x \rangle$ for the whole sample is independent of B.

The data of Fig. 11 also provide a possible resolution of a controversy in the literature concerning the magnitude of the LMR in single-crystal Al when **B** is directed along the [110] crystal axis. Kesternich, Ullmaier, and Schilling[15] reported an unusually large LMR ($S=2.4\times10^{-2}$) for a single crystal of Al when a magnetic field was oriented along the [110] axis. Their measurements were made using a four-probe technique with long, thin samples such as ours. The large LMR's were very sensitive to orientation, dropping off rapidly as B was moved away from [110]. Kesternich, Ullmaier, and Schilling attributed the large LMR to magnetic breakdown along [110]. Datars and Douglas[20] attempted to reproduce this large LMR using a probeless technique on spherical samples, without success. They found a much smaller enhancement along [110], and concluded that the effect reported by Kesternich, Ullmaier, and Schilling could not be intrinsic to Al. To date, no resolution of this discrepancy has been proposed.

A possible resolution lies in the shape of the sample used by Kesternich, Ullmaier, and Schilling. Figure 1 of Ref. 15 shows that their sample had arms similar to those of our samples, and that their arms pointed exactly along the [110] crystal direction. Thus when **B** was parallel to [110] it pointed directly along the arms. Moreover, S for the Kesternich, Ullmaier, and Schilling sample was about equal to the upper bound predicted by Eq. (25). It thus seems likely that a substantial portion of the large LMR they saw for **B**||[110] was due to a "surface-defect" contribution rather than to magnetic breakdown. The breakdown portion would then be much closer to the smaller LMR seen by Datars and Douglas, thereby greatly reducing the discrepancy.

C. Data not well understood

While our model provides a good description of the LMR when the magnetic field points directly along the potential arms of the sample, complexities arise regarding the angular variation of this LMR for very long, symmetrically located arms. Figure 14 shows results for different samples. For a symmetrical sample with short arms (arm length $\simeq L_y/2$), the LMR decreased monotonically with angle away from its maximum value at $\theta\simeq90°$ (i.e., **B** parallel to the arms). The maximum S for this

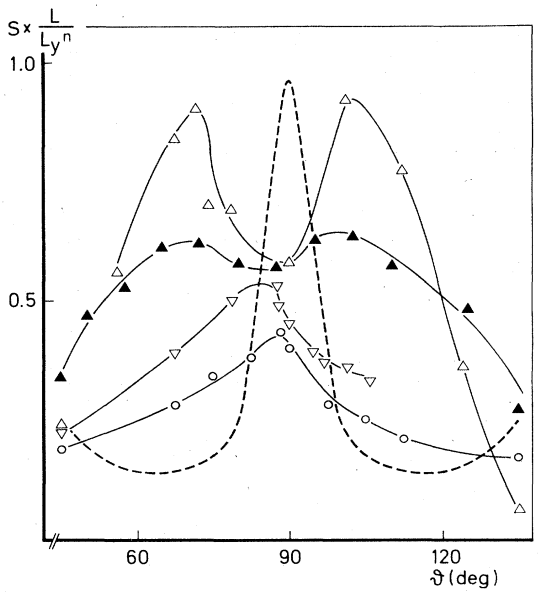

FIG. 14. Angular variation of transverse LMR for rotation in a magnetic field for symmetrical samples (having only pairs of oppositely placed arms) and asymmetrical samples (having also unpaired arms). In addition, there are samples with long arms (4 times longer than the sample width L_y) or short arms (shorter than L_y). $\theta=90°$ means **B** directed along arms. The LMR is expressed in $S(L/L_yn)$, where L is the distance between voltage contacts, L_y is the width of the sample, and n is the number of pairs of opposite arms plus the number of unpaired arms between voltage contacts with the voltage contacts themselves counting together as one additional arm. S is the electrical or thermal Kohler slope: electric, $S=(1/R_H)(\partial\rho/\partial B)$, where R_H is the Hall coefficient, and thermal, $S=(1/A_{\mathrm{RL}})(\partial\rho/\partial B)$, where A_{RL} is the Righi-Leduc coefficient. Dashed line: Asymmetric sample, long arms, electrical LMR, from Ref. 12. Upright open triangles: Symmetric sample, long arms, electrical LMR. Inverted open triangles: Symmetric sample, short arms, electrical LMR. Upright open triangles: Symmetric sample, long arms, thermal LMR. Open circles: Asymmetric sample, long arms, electrical LMR. The lines are only to guide the eyes, they are not the results of any calculations.

sample was approximately half the maximum predicted by Eq. (25). Similar behavior was observed in an asymmetric sample (with unpaired arms) with long arms (arm length $\simeq3.5L_y$). On the other hand, a symmetric sample with long arms (arm length $\simeq3.5L_y$), displayed an unexpected *non*monotonic variation of LMR with angle, which was also manifest in the thermal magnetoresistance of a sample of similar shape. It is interesting to note that the size of the LMR at parallel orientation (90°) is nearly the same for all four samples; it is thus only the behavior away from parallel which is "anomalous."

For comparison, the dashed line shows data for the sample of Kesternich, Ullmaier, and Schilling.[12] Its LMR at 90° is higher than that of our samples, and drops off more rapidly with angle away from 90°. Their sample shapes was intermediate between our symmetric and

asymmetric samples, with much smaller thickness.

To ascertain how important it is to the LMR that surface defects extend completely across the sample, we made a few observations on grooves and one projection which extended only part way across the sample width. In such a case, the last term on the left-hand side of Eq. (14) is no longer zero and we may not have a rotation-free average electric field.

The results can be summarized as follows:

When **B** was directed perpendicular to the sample surfaces the LMR for the partial defects was always considerably smaller than the LMR for a full defect of the same depth (height).

The LMR for partial defects was an asymmetric function of angle as **B** was rotated away from the perpendicular to the sample plane (i.e., away from $\theta=0$). The asymmetry was particularly pronounced for a defect which extended nearly all the way across the sample width.

Finally, we describe some changes observed in the LMR of samples upon annealing. The most reproducible result was that the LMR for flat portions of a sample always decreased upon annealing, typically by 50% or more. This behavior is consistent with the suggestion made in Sec. II above that different sources of LMR—here dislocations and whatever else is present—might be simply additive in their effect. In contrast, the raw-data LMR's for grooves or projections usually increased upon annealing, but sometimes decreased. Such divergent behavior is not what would be expected for simple additivity. When "net" LMR's were calculated by subtracting out the LMR's for flat pieces on the same annealed or unannealed sample, then these "net" LMR's almost always increased upon annealing. We currently have no explanation for the increase in "net" LMR generally observed upon sample annealing.

V. SUMMARY AND CONCLUSIONS

We have presented here a model of surface-induced transverse magnetoresistance in metallic plates, and shown that this model describes quantitatively the magnetoresistance observed for well-annealed aluminum plates in the form of wedge-shaped samples, samples with surface steps, and samples with grooves or projections which extend completely across the sample width. The physical source of the magnetoresistance lies in the fact that the averaged electric field in the plates is essentially rotation free. This forces differences in Hall voltage at places of different sample thickness to appear along the length of the sample, thereby generating a large magnetoresistance. We showed that this magnetoresistance is larger than that obtained by applying to surface defects the standard theory of LMR for volume defects. The following observations are in accord with our model.

(1) Direct measurements of Hall voltage difference between portions of the sample having different thicknesses showed that these differences increased linearly with magnetic field strength B and were in good agreement with magnetoresistance voltages measured along the sample length.

(2) As predicted by our model, the magnetic-field-induced voltages on opposite sides of both a wedge-shaped sample and a sample containing a step defect were asymmetric and not strictly linear in B. They were also in quantitative agreement with the predicted magnitude.

(3) As predicted by our model, the magnetoresistance observed with grooves (projections) was linear in B and also directly proportional to the fractional groove (projection) depth (height), to the sample width and approximately to the number of defects per unit length of the sample. Again the observed magnitudes were in quantitative agreement with prediction.

(4) The effect of large surface defects on magnetoresistance was studied by rotating the sample 90° so that the magnetic field pointed along the sample arms. In such a case both a very large linear electric magnetoresistance and a very large linear thermal magnetoresistance was observed. These two magnetoresistances were related by the Wiedemann-Franz law and were within a factor of 2 of the large-defect limit predicted by our model.

Additional observations were made which are beyond the scope of our model and are not yet completely understood.

(1) When the magnetic field was rotated from the direction parallel to the sample arms toward the direction perpendicular to the arms, the magnetoresistance (electrical and thermal) for symmetrically shaped samples with long arms reached maximum values at intermediate angles.

(2) The magnetoresistance observed with grooves (projections) extending only part way across the sample were generally smaller than those for grooves (projections) of the same depth (height) extending all the way across, and were sometimes a highly asymmetric function of angle when the magnetic field was rotated.

(3) The magnetoresistance observed with grooves (projections) in unannealed samples was usually smaller than those in equivalent annealed samples, and showed larger variations under similar conditions.

We conclude that our model provides a very good description of those magnetoresistance observations to which it is applicable, especially data for grooves (projections) of fractional depth (height) Δ extending completely across a sample. For a sample of width L_y and length between potential leads, L, the model predicts a dimensionless Kohler slope for the linear magnetoresistance of

$$S=\frac{L_y}{L}\Delta\ .$$

This means that for $L_y \simeq L$, a single groove or projection with $\Delta \simeq 10^{-3}$ will produce $S \simeq 10^{-3}$, which is comparable to the smallest LMR reported in the literature for simple metals such as aluminum. Surface defects thus are likely to have played a significant role in many reported observations of linear magnetoresistance in simple metals.

ACKNOWLEDGMENTS

Part of this work has been supported by the "Stichting voor Fundamenteel Onderzoek der Materie" (FOM) with financial support from the "Nederlandse Organisatie voor Zuiver Wetenschappelijk Onderzoek" (ZWO). The au-

thors wish to thank Drs. J. Meyers for his contribution to the thermal measurements. One of us (J.B.) wants to thank the University of Nijmegen for hospitality during various stages of the research. Participation of J.B. in this research was made possible in part by support from the U.S. National Science Foundation through Grant No. DMR-83-03206 and also from the North Atlantic Treaty Organization through Travel Grant No. 1956.

---

*Permanent address: Physics Department, Michigan State University, E. Lansing, MI 48824.

†Present address: Max-Planck-Institut für Festkörperforschung, Hochfeld-Magnetlabor, 166x, F-38042 Grenoble-Cedex, France.

[1]I. M. Lifshitz, M. Ya. Azbel, and M. I. Kaganov, Zh. Eksp. Teor. Fiz. **31**, 63 (1956) [Sov. Phys.—JETP **4**, 41 (1957)].

[2]A. W. Overhauser, Adv. Phys. **27**, 343 (1978).

[3]V. I. Gostishchev, A. A. Drozd, and S. E. Dem'yanov, Fiz. Nizk. Temp. **44**, 1131 (1978) [Sov. J. Low Temp. Phys. **4**, 532 (1978)].

[4]T. Amundsen and P. Jerstad, J. Low Temp. Phys. **15**, 459 (1974).

[5]D. Stroud and F. P. Pan, Phys. Rev. B **13**, 1434 (1976).

[6]J. B. Sampsel and J. C. Garland, Phys. Rev. B **13**, 583 (1976).

[7]A. P. van Gelder (unpublished).

[8]C. J. Beers, J. C. M. van Dongen, H. van Kempen, and P. Wyder, Phys. Rev. Lett. **40**, 1194 (1978).

[9]K. Yoshida, J. Phys. F **11**, L245 (1981).

[10]G. J. C. L. Bruls, J. Bass, A. P. van Gelder, H. van Kempen, and P. Wyder, Phys. Rev. Lett. **46**, 553 (1981).

[11]R. T. Bate and A. C. Beer, J. Appl. Phys. **32**, 800 (1961).

[12]R. T. Bate, J. C. Bell, and A. C. Beer, J. Appl. Phys. **32**, 806 (1961).

[13]M. Abramowitz and I. A. Stegun, *Handbook of Mathematical Functions* (Dover, New York, 1965).

[14]F. R. Fickett, Phys. Rev. B **3**, 1941 (1971).

[15]W. Kesternich, H. Ullmaier, and W. Schilling, Philos. Mag. **31**, 471 (1975).

[16]Vereinigte Aluminium Werke AG, Postfach 2468, 5300 Bonn 1, FGR.

[17]The statement in Ref. 10 that we "always" measured both $V_{AA'}$ and $V_{CC'}$ was erroneous, and is hereby corrected.

[18]Tekelec Airtronic SA, DC Digital Voltmeter TE 925, Sèvres, France.

[19]J. Meyers, Doctoral thesis, University of Nijmegen, 1982.

[20]R. J. Datars and W. R. Douglas, Solid State Commun. **14**, 461 (1974).